ARCHIVES
of
FOUNDRY ENGINEERING

ISSN (2299-2944)

10.24425/afe.2025.155357

Published quarterly as the organ of the Foundry Commission of the Polish Academy of Sciences

Evaluation of the Quality of the Connection Between ZrO_2-Y_2O_3 Coating With NiAl Interlayer and AlSi7Mg Alloy Casting Using the Scratch Test Method

M.F. Mróz, P. Rąb *
Rzeszow University of Technology, Rzeszów, Poland
* Corresponding author. e-mail address: p.rab@prz.edu.pl

Received 08.01.2025; accepted in revised form 10.03.2025; available online 23.07.2025

Abstract

This article presents an evaluation of the quality of the connection between the ZrO2-Y2O3 coating with the NiAl interlayer and AlSi7Mg alloy casting, utilising the scratch test method. The study analysed the ZrO2-Y2O3 coating with the NiAl interlayer applied using the APS (Atmospheric Plasma Spraying) method. The chemical composition of the zirconia coating and the interlayer was analysed. The core element of the study involves scratch test examinations of the analysed coatings, determining their scratch resistance. Scanning electron microscopy was used to analyse the scratch area to identify any potential cracks or delaminations at the casting-NiAl interlayer boundary, and the NiAl interlayer-ZrO2-Y2O3 coating boundary. Based on the conducted studies, high-quality connection of the ZrO2-Y2O3 coating with the NiAl interlayer and the AlSi7Mg alloy casting was concluded. The results of these studies will form the basis for further work on the application of TBC (Thermal Barrier Coating) to improve the operational durability of aluminium alloy parts working under high-temperature conditions.

Keywords: AlSi7Mg alloy, Atmospheric plasma spraying, Thermal barrier coating, ZrO2-Y2O3, NiAl

1. Introduction

Due to their low density, good strength-to-weight ratio, low thermal expansion coefficient, and good corrosion resistance, aluminium-silicon alloys are widely used for machine parts and components [1,2]. These alloys, due to their good mechanical and casting properties, have found applications in the aerospace and automotive industries, including engine components such as engine blocks, pistons, and cylinder heads [3-5].

In the engine chamber, where variable conditions are caused by the combustion of the fuel-air mixture, interacting components like pistons and heads are exposed to high temperature, pressure, and thermal shock, which can lead to damage [6-9].

The authors of [10] claim that the upper surface of the piston made of aluminium-silicon alloy can melt over time, which, under conditions of rapid cooling, can lead to cracking. Similar conclusions were reached by the authors of [11], who noted that in the area of the thin walls of valve seats, large stresses resulting from the thermal load caused by the engine's work cycle and combustion of the mixture can lead to cracking.

One solution to improve the operational durability of engine components is the use of TBC coatings [12-15]. TBC coatings, characterised by low thermal conductivity, create an insulating

layer between the hot zone of the engine, caused by the combustion of the fuel-air mixture, and the engine components. Research results by [16,17] confirm that the use of these coatings improves the longevity of components working at elevated temperatures and reduces gas emissions produced in the combustion chamber. Additionally, the authors of [18] state that the application of TBC coatings, besides improving the operational durability of the engine, increases its power and reduces fuel consumption without significant design modifications to the internal combustion engine.

The purpose of this study was to evaluate the quality of the connection between the ZrO2-Y2O3 coating with the NiAl interlayer and the AlSi7Mg alloy casting using the scratch test method. The study analysed the ZrO2-Y2O3 coating with the interlayer, which was applied using the APS method. The microstructure and chemical composition of the substrate material and coatings were analysed. The quality assessment of the connection between the NiAl interlayer and the AlSi7Mg alloy substrate, as well as the ZrO2-Y2O3 coating, was performed using the scratch test method.

2. Research Material and Methodology

The material for the study was a casting of AlSi7Mg alloy. The chemical composition analysis was performed using a Tasman Q4 emission spectrometer by Bruker. The results of this analysis are shown in Table 1.

Table 1.
The results of the chemical composition analysis of the AlSi7Mg alloy.

Si, %	Mg, %	Mn, %	Fe, %	Al, %
6.98	0.27	0.01	0.11	Rest

The microstructure of the AlSi7Mg alloy is shown in Figure 1. It is a typical hypoeutectic silumin microstructure, consisting of primary dendrites of the α(Al) phase and an interdentritic eutectic α(Al)+β(Si) distribution. Observation of this alloy's microstructure also revealed the presence of bright precipitates in the eutectic region. To identify these precipitates, X-ray microanalysis of the chemical composition was performed (Figure 2). The results, shown in the table below the figure, indicate that these are iron-rich intermetallic phases.

Two types of powders were used to produce the coatings. The first was used to produce the NiAl interlayer, and the second for the ZrO2-Y2O3 coating. The NiAl interlayer was produced using Metco 404NS powder, which contains 80% Ni, with the remainder being aluminium.

The appearance of NiAl powder particles is shown in Figure 3. The powder consisted of rounded grains ranging from 45 to 120 µm in size. The chemical composition analysis of this powder (Figure 4) confirmed that it primarily contains nickel and aluminium.

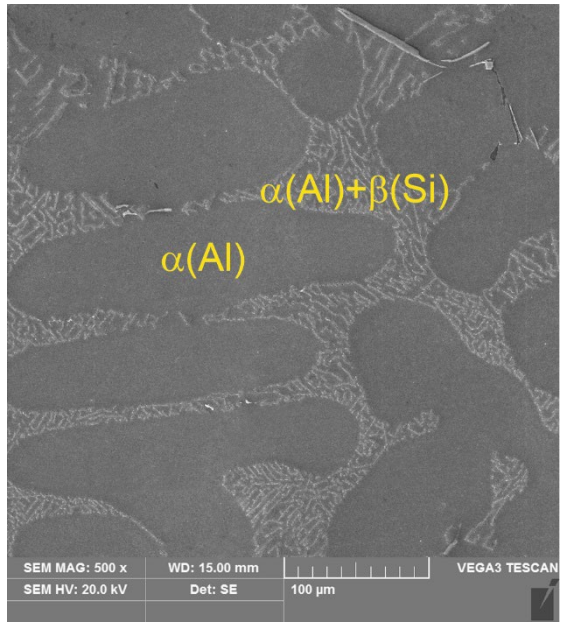

Fig. 1. SEM image of the typical microstructure of AlSi7Mg alloy with marked α and β phases

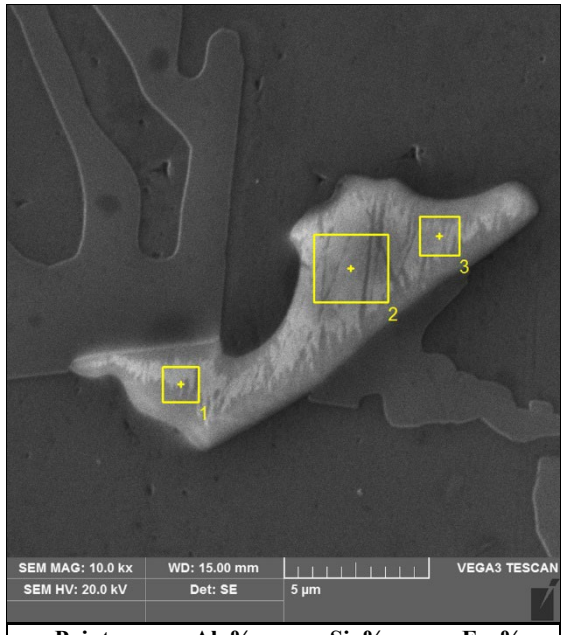

Point	Al, %	Si, %	Fe, %
1	61.35	14.21	24.44
2	63.81	11.06	25.12
3	67.10	10.65	22.25

Fig. 2. Results of X-ray microanalysis of intermetallic phases in the microstructure AlSi7Mg alloy

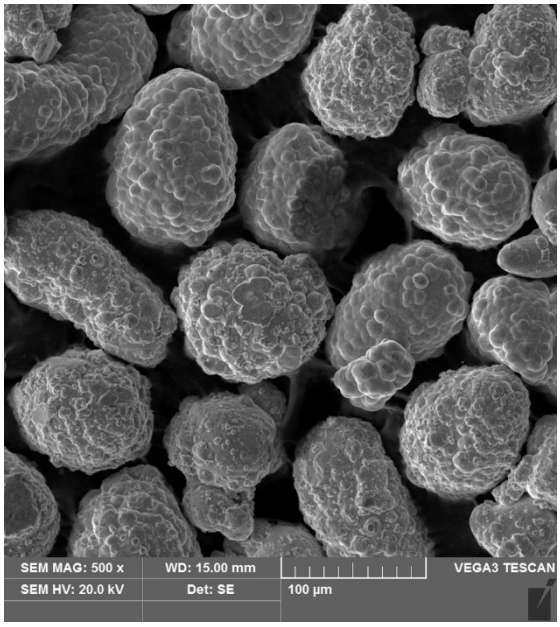

Fig. 3. SEM image of NiAl powder

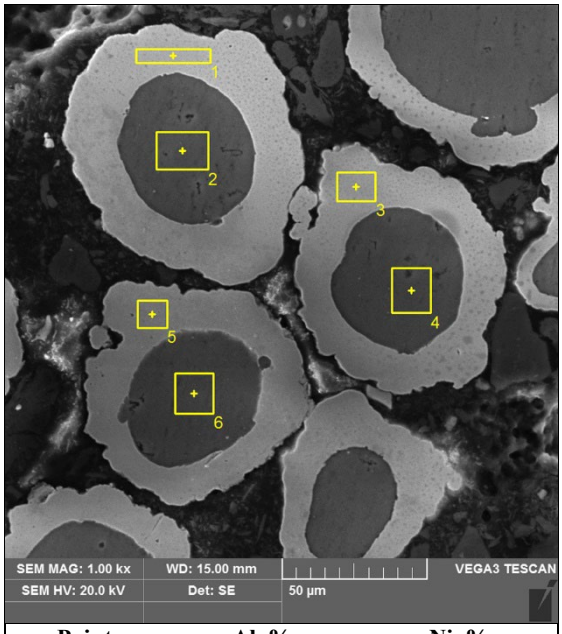

Point	Al, %	Ni, %
1	0.30	99.70
2	98.78	1.22
3	0.30	99.70
4	98.75	1.25
5	0.32	99.68
6	98.58	1.42

Fig. 4. Results of X-ray microanalysis of NiAl powder

For producing the ZrO2-Y2O3 coating on the NiAl interlayer, Saint-Gobain #204 powder was used. This powder contained 92% ZrO2 and 8% Y2O3. The appearance of ZrO2-Y2O3 powder particles is shown in Figure 5. The powder consisted of spherical grains with diameters ranging from 25 to 95 µm and a small amount of finer particles. The results of the analysis of Saint-Gobain #204 powder are shown in Figure 6.

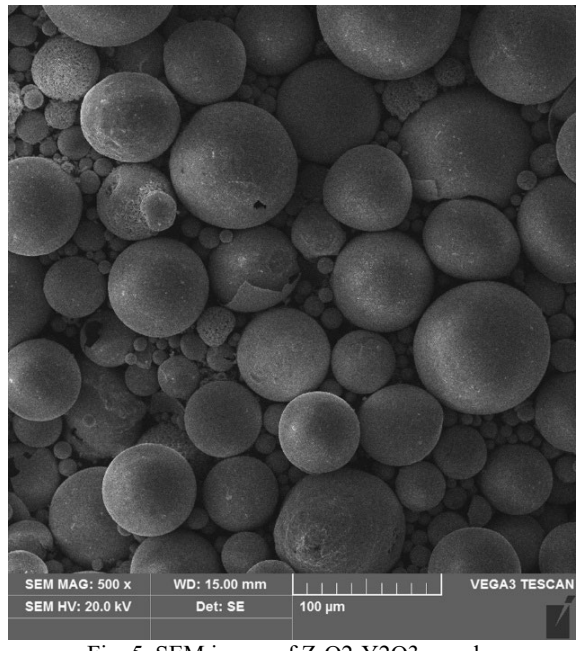

Fig. 5. SEM image of ZrO2-Y2O3 powder

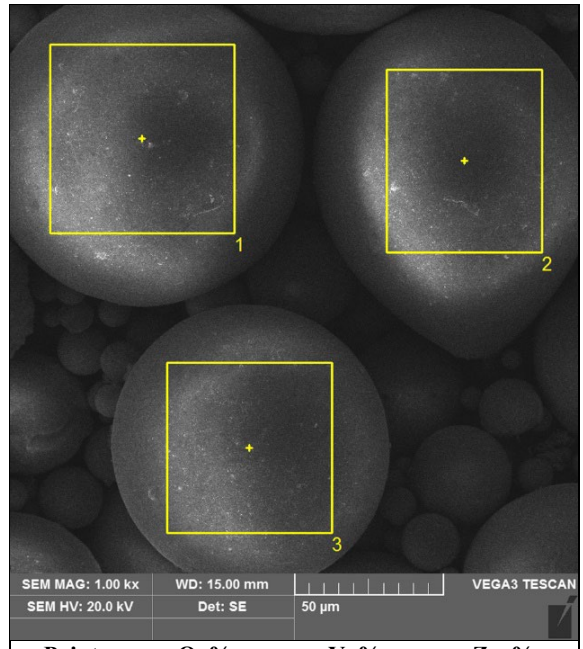

Point	O, %	Y, %	Zr, %
1	30.38	4.15	65.47
2	29.66	4.19	66.15
3	29.94	3.63	66.43

Fig. 6. Results of X-ray microanalysis of ZrO2-Y2O3 powder

The coating application process was carried out using the APS method with a Sulzer F4-MB-HBS torch. The parameters for applying the NiAl and ZrO2-Y2O3 coatings are presented in Table 2. Before applying the coating, the AlSi7Mg alloy substrate material underwent abrasive blasting to increase the surface roughness, ensuring better adhesion of the coating to the substrate. After this treatment, the substrate was degreased using acetone in an ultrasonic cleaner.

Table 2.
Parameters for applying the intermediate and main coatings.

Process parameters	**Values**	
Powder type	NiAl	ZrO2-Y2O3
Carrier gas, l/min	4	3
Feeder disk speed, %	5	5
Current intensity, A	620	620
Plasma-generating gas Ar, l/min	30	35
Plasma-generating gas H2, l/min	5.2	8
Air jet – air, bar	3	4
Spraying distance, mm	100	120
Torch speed, mm/min	200	200
Layer thickness, µm	120-200	280-350
Number of torch passes	10	20

The appearance of the coating surface after the APS spraying process is shown in Figure 7.

Microstructure observation was conducted on metallographic specimens. To reveal the microstructure, the sections were etched with a 5% hydrofluoric acid solution.

Microstructure studies and X-ray chemical composition analysis were performed using a TESCAN Vega 3 scanning electron microscope equipped with an INCA X-ACT (OXFORD) module.

To assess the quality of the bond between the substrate and the NiAl interlayer, as well as between the NiAl interlayer and the ZrO2-Y2O3 coating, scratches were made using a Scratch Tester Revetest RST. Scratches were made from the substrate material (AlSi7Mg alloy) to the ZrO2-Y2O3 coating over a length of 1 mm. A constant Rockwell indenter load of 5N was applied. The scratching speed was 5 mm/min.

Fig. 7. Surface appearance of the ZrO2-Y2O3 coating on AlSi7Mg alloy casting after APS spraying

3. Results and Analysis

An example of the coating applied to the AlSi7Mg alloy casting is shown in Figure 8.

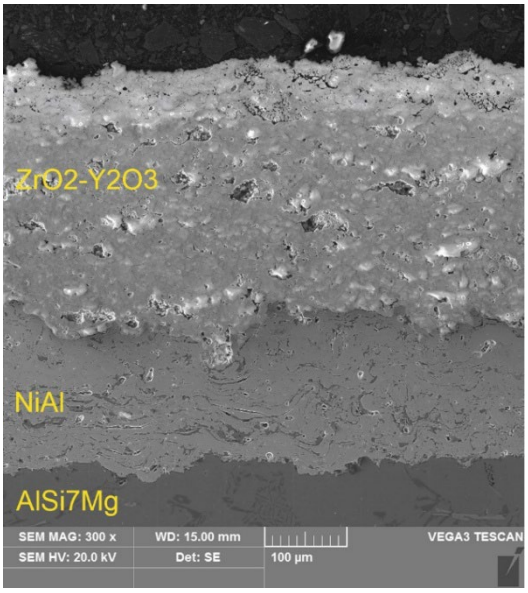

Fig. 8. SEM image of ZrO2-Y2O3 coating with NiAl interlayer on AlSi7Mg alloy casting

Analysis of the bond between the NiAl interlayer and the AlSi7Mg alloy substrate showed no delaminations or cracks and a high degree of development of the bonding line, characterised by characteristic anchorages (Figure 9). No cracks or delaminations were also found at the NiAl interlayer-ZrO2-Y2O3 coating boundary, indicating very good adhesion of the ZrO2-Y2O3 coating to the interlayer.

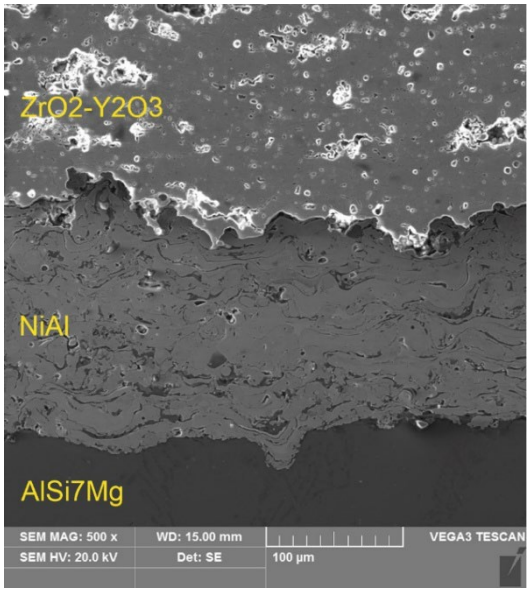

Fig. 9. SEM image of ZrO2-Y2O3 coating with NiAl interlayer on AlSi7Mg alloy casting with characteristic anchorages

Figures 10 and 11 present the results of the chemical composition analysis of the NiAl interlayer and the ZrO2-Y2O3 coating.

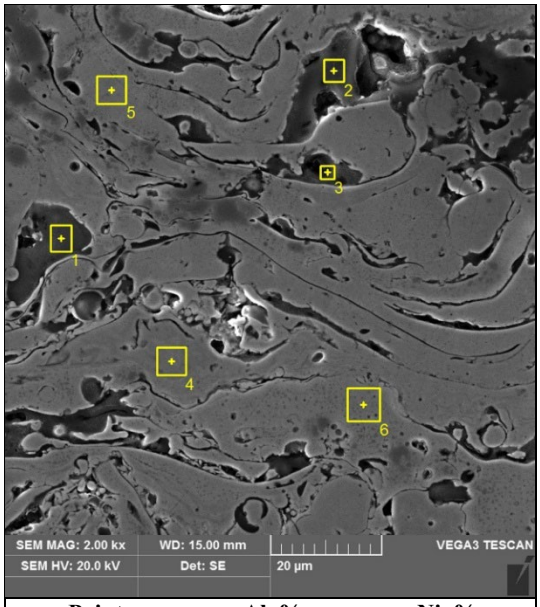

Point	Al, %	Ni, %
1	94.56	5.44
2	8.04	91.96
3	96.42	3.58
4	46.97	53.03
5	7.03	92.97
6	0.62	99.38

Fig. 10. Results of X-ray microanalysis of the chemical composition of the NiAl coating

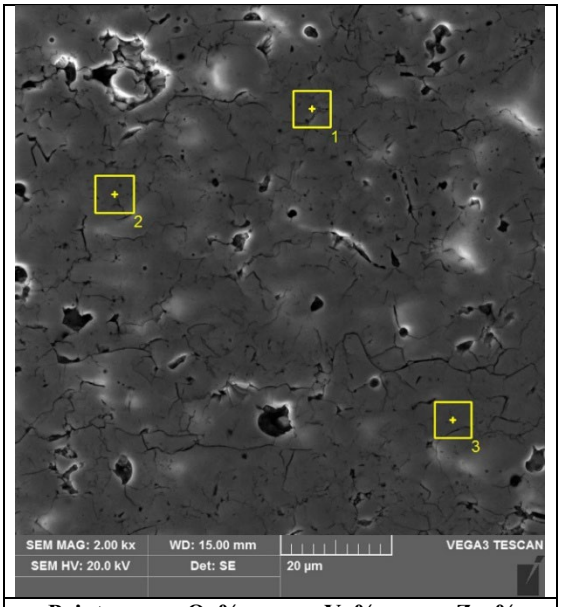

Point	O, %	Y, %	Zr, %
1	27.35	4.86	67.79
2	27.44	4.36	68.19
3	27.63	4.46	67.91

Fig. 11. Results of X-ray microanalysis of the chemical composition of the ZrO2-Y2O3 coating

In the interlayer, there are aluminium and nickel particles that have melted or fully fused in the plasma arc stream. The coating contains particles of zirconium oxide and yttrium oxide, which are fully or partially melted in the plasma arc stream.

The results of the scratch test are presented in Figure 12 and 13. During the scratch test, the indenter penetration depth, friction force, normal force, friction coefficient, and acoustic emission (EA) signal were analysed. Table 3 and Figure 12 present the results of measuring the scratch depth and width in the substrate and coating.

The obtained results indicate that the ZrO2-Y2O3 coating has the smallest scratch width and depth values. Significant differences were observed in the indenter penetration width values. For the ZrO2-Y2O3 coating, the scratch width is more than three times smaller than the scratch width in the AlSi7Mg substrate. The scratch width in the NiAl interlayer is nearly half that in the substrate.

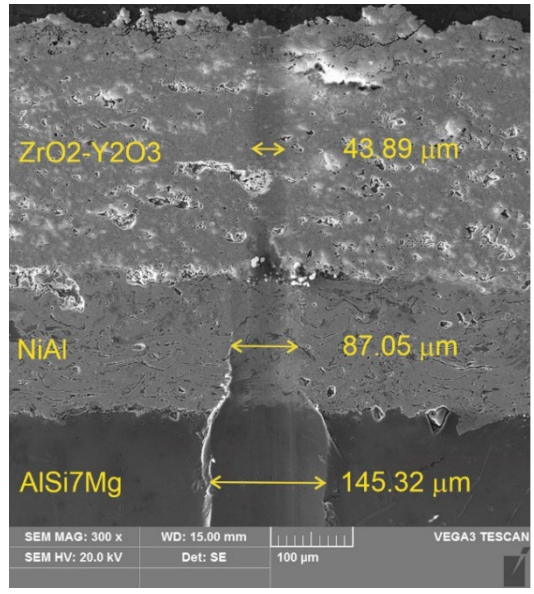

Fig. 12. SEM image and scratch width measurement results in the transition area from the AlSi7Mg substrate to the NiAl interlayer and from the NiAl interlayer to the ZrO2-Y2O3 coating

Table 3.
Scratch geometry parameters of the substrate and coating (Figure 12)

Area	Value, µm	
	Depth	Width
Substrate	5.47-5.75	145.32
NiAl coating	4.65-5.06	87.05
ZrO2-Y2O3 coating	3.83-4.14	43.89

The analysis of transition areas from the substrate to the NiAl interlayer and from the NiAl interlayer to the ZrO2-Y2O3 coating did not reveal the presence of cracks or delaminations. Only in the transition area from the NiAl interlayer to the ZrO2-Y2O3 coating was there a cluster of small particles, likely formed due to the degradation of the ZrO2-Y2O3 layer at the moment when the indenter began to penetrate this layer (Figure 14).

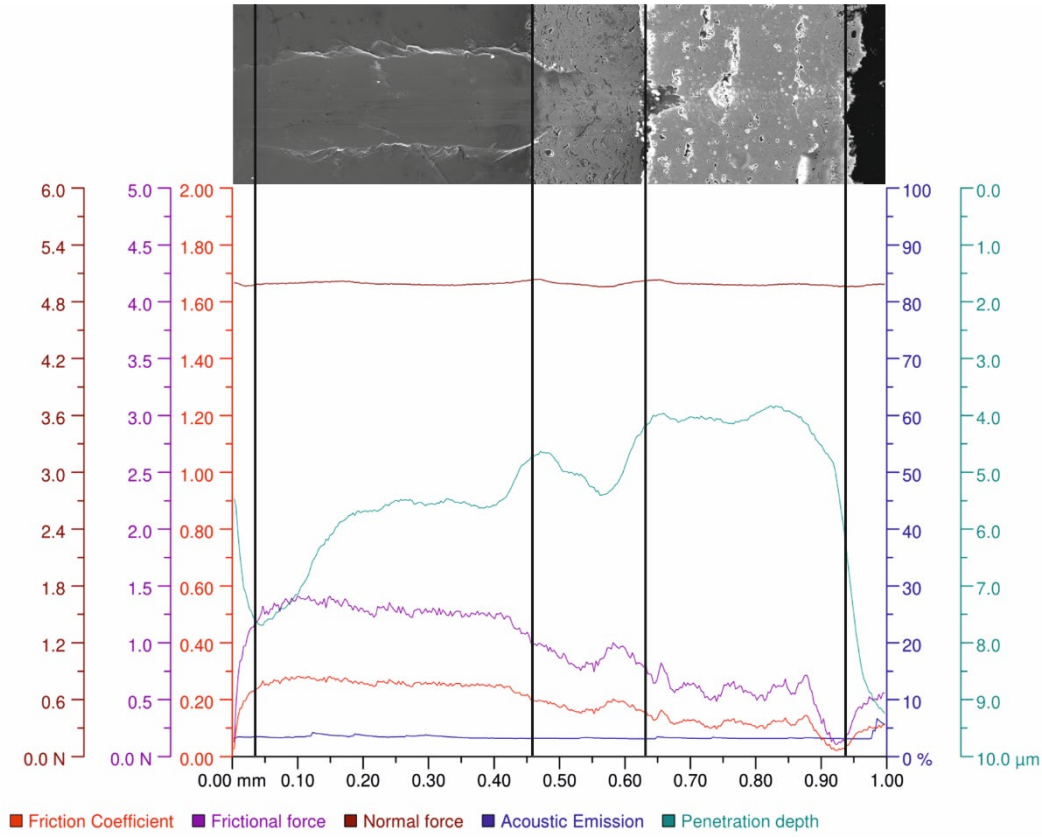

Fig. 13. Scratch test parameter progression during the scratching of the substrate material, NiAl coating, and ZrO2-Y2O3 coating

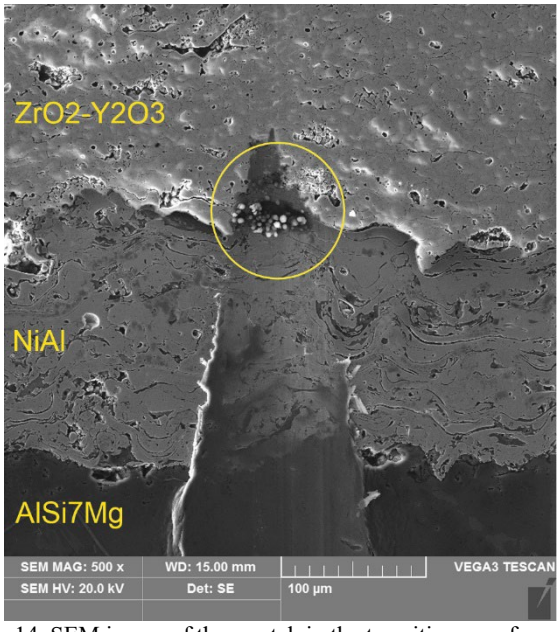

Fig. 14. SEM image of the scratch in the transition area from the AlSi7Mg substrate to the NiAl interlayer and from the NiAl interlayer to the ZrO2-Y2O3 coating

4. Conclusions

The obtained research results indicate that there are no delaminations or cracks in the scratch area at the transition boundary from the AlSi7Mg alloy substrate to the NiAl interlayer and from the NiAl interlayer to the ZrO2-Y2O3 coating. Significant differences were found in the scratch width values and in the indenter penetration depth, indicating different scratch resistances of the substrate and the ZrO2-Y2O3 coating with the NiAl interlayer. In the scratch area at the transition boundary from the NiAl interlayer to the ZrO2-Y2O3 coating, clusters of small particles were observed, suggesting they resulted from the degradation of the ZrO2-Y2O3 coating at the moment scratching began.

The presented research results represent the first stage of extensive studies on the potential application of zirconium coatings to improve the operational durability of components working at elevated temperatures.

References

[1] Petrič, M., Zeka, B., Mrvar, P., Nagode, A., Vončina, M. & Balaško, T. (2022). Solidification behaviour and microstructure of AlSi7Mg cast alloy with addition of Li.

Journal of Materials Research and Technology. 19, 2084-2092. https://doi.org/10.1016/j.jmrt.2022.05.171.
[2] Pezda, J. (2022). Optimization of heat treatment parameters of AlSi7Mg alloy. *Materials*. 15(3), 1163, 1-16. https://doi.org/10.3390/ma15031163.
[3] Timelli, G., Camicia, G., Ferraro, S. & Molina, R. (2014). Effects of grain refinement on the microstructure, mechanical properties and reliability of AlSi7Cu3Mg gravity die cast cylinder heads. *Metals and Materials International*. 20, 677-686. https://doi.org/10.1007/s12540-014-4013-2.
[4] Dyzia, M. (2017). Aluminum matrix composite (AlSi7Mg2Sr0. 03/SiCp) pistons obtained by mechanical mixing method. *Materials*. 11(1), 42, 1-14. https://doi.org/10.3390/ma11010042.
[5] Siadkowska, K. & Czyż, Z. (2019). Selecting a material for an aircraft diesel engine block. *Combustion Engines*. 58(3), 4-8. http://dx.doi.org/10.19206/CE-2019-301.
[6] Natesan, E., Meyer, K. A., Eriksson, S., Ahlström, J. & Persson, C. (2020). Effects of dwell time on the deformation and fatigue behaviour of A356-T7 cast aluminium alloys used in high specific power IC engine cylinder heads. *Materials.* 13(12), 2727, 1-27. https://doi.org/10.3390/ma13122727.
[7] Kumar, D. & Pandey, K.N. (2014). Study on thermal fatigue behavior of plasma sprayed yttria zirconia thermal barrier coatings (TBCs) systems on aluminum alloy. *International Journal of Mechanical and Production Engineering*. 2(3), 19-22. ISSN: 2320-2092. http://dx.doi.org/10.13140/2.1.1302.9769.
[8] Sharma, P., Dwivedi, V.K. & Kumar, D. (2020). Effect of shape on the mechanical properties of thermal barrier coating of YSZ7-8. *Materials Today: Proceedings*. 26(2), 1921-1925. DOI: https://doi.org/10.1016/j.matpr.2020.02.420.
[9] Kumar, D., Dwivedi, V.K. & Saraswat, A. (2022). Performance of 2024 aluminum alloy thermal barrier coating systems subjected to elevated temperature fluctuation as a fatigue. *Sādhanā*. 47(4), 216. https://doi.org/10.1007/s12046-022-01996-y.
[10] Brusa, A., Cavina, N., Rojo, N., Mecagni, J., Corti, E., Ravaglioli, V., Cucchi, M. & Silvestri, N. (2021). Development and experimental validation of an adaptive, piston-damage-based combustion control system for Si engines: Part 1—evaluating open-loop chain performance. *Energies*. 14(17), 5367. https://doi.org/10.3390/en14175367.
[11] Azadi, M., Mafi, A., Roozban, M. & Moghaddam, F. (2012). Failure analysis of a cracked gasoline engine cylinder head. *Journal of Failure Analysis and Prevention*. 12, 286-294. https://doi.org/10.1007/s11668-012-9560-6.
[12] Mróz, M. & Rąb, P. (2023). Evaluation of the Possibility of Applying Thermal Barrier Coatings to AlSi7Mg Alloy Castings. *Archives of Foundry Engineering*. 23(3), 104-109. https://doi.org/10.24425/afe.2023.146668.
[13] Bellippady, M., Björklund, S., Li, X.H., Frykholm, R., Kjellman, B., Joshi, S. & Markocsan, N. (2024). Performance of atmospheric plasma-sprayed thermal barrier coatings on additively manufactured super alloy substrates. *Coatings*. 14(5), 626, 1-17. https://doi.org/10.3390/coatings14050626
[14] Sharma, P., Dwivedi, V.K. & Kumar, D. (2022). Characterisation of anode plasma deposited IN718 TBC system after thermal cycle shocking test. *Advances in Materials and Processing Technologies.* 8(sup2), 861-869. https://doi.org/10.1080/2374068X.2021.1948711.
[15] Sharma, P., Dwivedi, V.K. & Kumar, D. (2021). A comparative analysis of different techniques of thermal barrier coating. In Recent Trends in Industrial and Production Engineering: Select Proceedings of ICAST 2020 (pp. 1-10). Springer Singapore. DOI: https://doi.org/10.1007/978-981-16-3135-1_1.
[16] Taymaz, I. (2007). The effect of thermal barrier coatings on diesel engine performance. *Surface and Coatings Technology*. 201(9-11), 5249-5252. https://doi.org/10.1016/j.surfcoat.2006.07.123.
[17] Liu, Y., Lei, J., Deng, X., Liu, Y., Sun, D. & Zhang, Y. (2023). Research and analysis of a thermal optimisation design method for aluminium alloy pistons in diesel engines. *Case Studies in Thermal Engineering*. 52, 103667, 1-14. https://doi.org/10.1016/j.csite.2023.103667.
[18] Hazar, H. & Ozturk, U. (2010). The effects of Al2O3–TiO2 coating in a diesel engine on performance and emission of corn oil methyl ester. *Renewable Energy*. 35(10), 2211-2216. DOI: https://doi.org/10.1016/j.renene.2010.02.028.